Backbiting and β-Scission Reactions in Free-Radical Polymerization of Methyl Acrylate

Shi Liu,[a] Sriraj Srinivasan,[b] Michael C. Grady,[c] Masoud Soroush,[d] and Andrew M. Rappe[a]*

Multiple mechanisms of backbiting and β-scission reactions in free-radical polymerization of methyl acrylate are modeled using different levels of theory, and the rigid-rotor harmonic-oscillator (RRHO) and hindered-rotor (HR) approximations. We identify the most cost-effective computational method(s) for studying the reactions and assess the effects of different factors (e.g., functional type and chain length) on thermodynamic quantities, and then identify the most likely mechanisms with first-principles thermodynamic calculations and simulations of nuclear magnetic resonance (NMR) spectra. To this end, the composite method G4(MP2)-6X is used to calculate the energy barrier of a representative backbiting reaction. This calculated barrier is then compared with values obtained using density functional theory (DFT) (B3LYP, M06-2X, and PBE0) and a wavefunction-based quantum chemistry method (MP2) to establish the benchmark method. Our study reveals that the barriers predicted using B3LYP, M06-2X, and G4(MP2)-6X are comparable. The entropies calculated using the RRHO and HR approximations are also comparable. DFT calculations indicate that the 1:5 backbiting mechanism with a six-membered ring transition state and 1:7 backbiting with an eight-membered ring transition state are energetically more favored than 1:3 backbiting and 1:9 backbiting mechanisms. The thermodynamic favorability of 1:5 versus 1:7 backbiting depends on the live polymer chain length. The activation energies and rate constants of the left and right β-scission reactions are nearly equal. The calculated and experimental ^{13}C and ^{1}H NMR chemical shifts of polymer chains affected by backbiting and β-scission reactions agree with each other, which provides further evidence in favor of the proposed mechanisms. © 2013 Wiley Periodicals, Inc.

DOI: 10.1002/qua.24572

Introduction

Thermal free-radical polymerization of acrylates is used to manufacture a wide variety of paints, coatings, and adhesives.[1,2] In the last decade, stringent environmental regulations have lowered the volatile organic content in paint and coatings to <300 g/l. High-temperature (>100°C) polymerization processes replaced conventional low temperature processes, because acrylic resins with lower solvent content and lower molecular weight can be produced at higher temperatures.[3,4] Previous studies showed the occurrence of secondary reactions such as self-initiation,[3–5] backbiting, and β-scission reactions[6,7] in high-temperature polymerization of alkyl acrylates. Grady et al.[3] and Quan et al.[4] reported reproducible monomer conversions of 70–90% in homopolymerization and copolymerization of a class of alkyl acrylates and methacrylates at 120–200°C in the absence of any conventional thermal initiators. Density functional theory (DFT) studies[5,8,9] combined with experimental mass spectrometric analysis[10] revealed that the Flory mechanism is responsible for the monomer self-initiation at high temperatures. It was shown that two types of monoradicals (shown in Chart 1), monomeric monoradical (MMR), and dimeric monoradical (DMR), are the initiating species in the self-initiated homopolymerization of alkyl acrylates and methacrylates.[5,8–10]

The occurrence of intermolecular and intramolecular chain transfer reactions has been extensively studied in thermal polymerization of alkyl acrylates and methacrylates.[11,12] The postulated mechanisms of these reactions[12] are depicted in Figure 1. The chain transfer reactions involve the abstraction of a hydrogen atom from a tertiary carbon atom on the polymer backbone by a propagating radical to form a midchain radical (MCR). The MCR, a tertiary radical, further undergoes propagation, β-scission, or termination. It has been reported[11] that the intramolecular hydrogen transfer most likely prefers a six-membered ring transition state. However, no evidence of

[a] S. Liu, A. M. Rappe
Department of Chemistry, The Makineni Theoretical Laboratories, University of Pennsylvania, Philadelphia, Pennsylvania 19104-6323
E-mail: rappe@sas.upenn.edu
[b] S. Srinivasan
Arkema Inc, 900 First Avenue, King of Prussia, Pennsylvania 19406
[c] M. C. Grady
DuPont Experimental Station, Wilmington, Delaware 19880-0308
[d] M. Soroush
Department of Chemical and Biological Engineering, Drexel University, Pennsylvania 19104

Contract grant sponsor: National Science Foundation; contract grant numbers: CBET-1160169 and CBET-1159736.
Contract grant sponsor: National Science Foundation (S.L.); contract grant number: CBET-1159736.
Contract grant sponsor: Air Force Office of Scientific Research (A.M.R.); contract grant number: FA9550-10-1-0248.
Contract grant sponsor: National Science Foundation (M.S.); contract grant number: CBET-1160169.

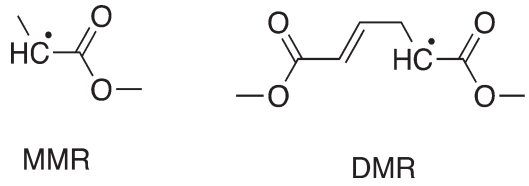

Chart 1. Structures of the monomeric monoradical (MMR) and dimeric monoradical (DMR) for methyl acrylate.

the existence of cyclic (six- or eight- or ten-membered ring) transition states in radical polymerization of acrylates is available as of yet. Monomer addition to MCRs is known to cause polymer chain branching.[13,14] Although higher (>50%) monomer concentration caused higher intermolecular chain transfer and long chain branching,[13] lower monomer concentration increased the occurrence of intramolecular chain transfer,[14] backbiting, and short chain branching.[15–17] Studies[4,15–21] using ^{13}C-nuclear magnetic resonance (^{13}C-NMR) spectroscopy showed the presence of linear and branched polymer chains in thermal polymerization of ethyl and *n*-butyl acrylate. It is noteworthy to point out that the NMR peaks corresponding to end-group substituents (ethyl and butyl) on each monomer unit can overlap with those of branch points on the polymer chain.[18] The existence of MCRs was detected via electron spin resonance.[19,20] Analysis revealed the existence of MCRs in *n*-BA radical polymerization at temperatures below 50°C.[21]

Previous studies determined that the β-scission reactions of the MCRs are more dominant at higher temperatures.[3,6,7,22] Figure 1 shows two possible pathways for the MCR fragmentation. The β-scission reaction leads to the formation of a secondary propagating radical (SPR) and a macromonomer. Yamada et al.[23] reported that the macromonomer, which has an unsaturated chain end (terminal double bond), can react with a radical and forms a SPR. Chiefari et al.[6] pointed out that the β-scission step at high temperatures can produce highly uniform macromonomers. Junkers et al.[7,22] carried out mass spectrometric studies and reported that a complex dynamic equilibrium between transfer and β-scission reactions is probably causing the formation of highly uniform macromonomers in the high-temperature autoinitiated (no initiator used) polymerization of *n*-butyl acrylate (*n*-BA). It was hypothesized[22] that the SPRs generated in β-scission reactions can further undergo backbiting reactions to produce additional MCRs. This results in a further decrease in the polymer chain length, a shift in the reaction equilibrium toward the formation of more MCRs and macromonomers, and the formation of polymer chains with a uniform chain distribution.

Pulsed-laser polymerization size-exclusion chromatography (PLP-SEC) is a benchmark approach that has been used to predict the kinetic rate constants of various reactions in free radical polymerization of alkyl acrylates. However, PLP-SEC has been unable to accurately determine the propagation rate coefficients in polymerization of *n*-BA at temperatures above 20°C due to the slow propagation and termination of MCRs.[11,24,25] The rate constants of various reactions in radical polymerization of acrylates have been estimated using a mechanistic model that fits simulated and experimental measurements such as monomer conversion, average molecular weights, and branching level.[24–31]

Wavefunction-based quantum chemical methods and DFT have been successfully applied to determine geometries of molecules, transition states, reaction mechanisms, and rate constants of initiation, propagation and chain transfer reactions in high temperature and controlled radical polymerization of acrylates and methacrylates.[5,8,9,32–39] Various DFT functionals have been successfully applied to study large polymeric systems.[33,37,40,41] It was shown that the 1:5 backbiting mechanism is preferred to 1:3 and 1:7 in thermal polymerization of acrylonitrile.[40] Degirmenci et al.[33] studied the propagation of methyl acrylate using B3LYP, MPW1K, BB1K, MPWB1K, and MPW1B95. More recently, hybrid functional B3LYP, pure functionals PBE, and TPSS, extensively parameterized functionals BMK and M06-2X, and long range and dispersion corrected functional wB97-XD, were used to determine the propagation rate constant of thermal polymerization of methyl acrylate.[41]

Recently, DFT calculations have been applied to explore the backbiting and β-scission reactions of acrylates.[42–45] Yu and Broadbelt[42] studied the 1:5 backbiting reactions in methyl acrylate and butyl acrylate with UB3LYP/6-31G** (MPWB1K/6-31G**) level of theory and reported an activation energy of 52.58 (59.94) kJ/mol and a frequency factor of 4.27×10^{12} (1.26×10^{13}) s^{-1} for methyl acrylate (*n*-butyl acrylate). We[43] studied different types of backbiting reactions in methyl acrylate with three density functionals, B3LYP, M06-2X, and PBE0, using a 6-31G* basis set. Our presented results indicated that 1:5 backbiting mechanism with a six-membered ring transition state and 1:7 backbiting with an eight-membered ring transition state are kinetically more favorable than 1:3 backbiting and 1:9 backbiting. Cuccato et al.[44] explored backbiting and β-scission reactions in *n*-butyl acrylate with a simplified molecular model in which side chains were replaced with hydrogen atoms. They concluded that 1:5 backbiting is the most favored mechanism. They[45] also considered a full-atomic terpolymer system composed of methyl acrylate, styrene, and methyl methacrylate to study backbiting, propagation, and β-scission reactions. Both the DFT-calculated activation energies and frequency factors for 1:5 backbiting reactions in previous studies (including our work)[42–45] are larger than "experimental" values[27,29,46] estimated using macroscopic mechanistic models, though the DFT-estimated rate constants are in reasonable agreement with the experimental values. In view of these efforts, there is a need to apply higher levels of theory to better understand the origin of the reported discrepancies. This article includes many new results obtained with higher-level quantum chemistry methods as well as our computational results presented at the 2012 AIChE Annual Meeting,[43] with the goal to distinguish the effect of different factors, such as the type of density functional, the size of basis set, approximations utilized for entropy calculation, and the chain length, on the calculated activation energies and frequency factors.

It should be noted that the accuracy of DFT depends on the approximation of the exchange-correlation function, and there is no systematic way to decide which density functional is the

best for a given type of chemical reaction. Wave-function-based quantum chemical methods directly approximate solutions to the Schrödinger equation, avoiding the DFT problems of finding and testing functionals. They can be systematically improved by increasing the basis set and/or including more electron configurations.[47] However, the computational cost of these wave-function-based methods are typically dramatically greater than that of DFT, which makes these methods impractical to use in the study of large polymer chains. For example, Møller–Plesset perturbation theory (MP2), the least expensive wave-function-based method that includes correlations, scales as N^5 (where N is the number of electrons); coupled cluster with single, double, and perturbative triple excitations, CCSD(T), which is considered the "gold standard" for chemical accuracy, scales as N^7.[48]

The composite quantum chemistry method G4(MP2)-6X.[49,50] combines high-level calculations (e.g., CCSD(T) with the complete basis set) and less-expensive low-level calculations. Benchmarking of the method that can produce energy barrier values comparable to G4(MP2)-6X is carried out by calculating the energy barrier of a representative backbiting reaction with G4(MP2)-6X, MP2, and DFT. Three types of density functionals, B3LYP, M06-2X, and PBE0, are employed in the benchmark study. In principle, other functionals optimized for kinetics, such as BB1K, BMK, and MPWB1K, could also be applied. Previously, benchmark studies have been carried out by Degirmenci et al.[33] (using BMK, BB1K, MPW1B95, MPW1K, and MPWB1K) and Yavuz et al.[41] (using B3LYP, PBE, TPSS, BMK, HSE2PBE, mPW1PW91, B97-1, wB97-xD, and M06-2X) for the propagation reaction of acrylates, which revealed that MPWB1K and M06-2X yield good qualitative agreement with experimental values of rate constants. The use of MPWB1K by Yu and Broadbelt[42] and Cuccato et al.[44,45] to study backbiting reactions of acrylates led us to apply M06-2X to prevent redundant work and compare the kinetic data obtained with B3LYP, PBE0, and M06-2X to those obtained with MPWB1K. Burke[47] recommended the use of "standard" density functionals, B3LYP for chemistry, and PBE0 for materials science, when exploring a new chemical system. We agree with this recommendation, because these two functionals have been used and tested extensively, and their advantages and disadvantages are better understood than other functionals. The B3LYP hybrid functional is described by:

$$E_{XC}^{B3LYP} = E_{XC}^{LDA} + \alpha_1(E_X^{HF} - E_X^{LDA}) + \alpha_2(E_X^{GGA} - E_X^{LDA}) + \alpha_3(E_C^{GGA} - E_C^{LDA}) \quad (1)$$

where LDA and GGA represent the local density approximation and the generalized gradient approximation. The three parameters, α_1, α_2, and α_3, are weights of the deviations of the exact Hartree–Fock exchange, GGA exchange, and GGA correlation from the LDA values. The weights are obtained by fitting to accurately computed thermochemical data.[51–53] B3LYP is widely used in chemistry and is considered a standard functional.[47] It is then a reasonable choice to assess the performance of B3LYP on those secondary reactions. M06-2X is a hybrid meta density functional, which incorporates kinetic-energy density in both the exchange and correlation functionals, and also has fitted weights.[54,55] M06-2X has been shown to predict accurate rate constants for radical propagation reactions of acrylates.[41] Its accuracy for backbiting and β-scission reactions is unknown as of yet. The hybrid density functional PBE0[56] is constructed semiempirically based on the nonempirical GGA functional and has a predefined weight of $^1/_4$ for the HF exchange term:

$$E_{XC}^{PBE0} = E_{XC}^{GGA} + \frac{1}{4}(E_X^{HF} - E_X^{GGA}) \quad (2)$$

PBE0 is in general a standard functional used in material science[47] and has been little used to study free radical polymerization of acrylates.

The accuracy of finite-temperature rate constants estimated using quantum chemistry methods depends on both the accuracy of the electronic-structure calculations and the approximations used for estimating activation entropy.[57,58] The rigid-rotor harmonic-oscillator (RRHO) approximation is widely used: the total partition function is decomposed into the product of translational, rotational, vibrational and electronic terms, and each normal mode is treated as a harmonic oscillator. The RRHO approximation is efficient and cost-effective, as simple analytical expressions are available for all the separated partition functions. However, when it is used for treating low frequency modes (that are mainly due to internal rotations), it predicts very inaccurate entropies and frequency factors.[59,60] The one-dimensional hindered-rotor (1D-HR) approximation has been shown to be a more suitable model for treating low-frequency torsional modes.[36,37,57,58] The application of the 1D-HR approximation requires the knowledge of the full rotational potential for each low frequency mode, which turns to be an expensive method for large polymer systems. We applied the RRHO and 1D-HR approximations and compared their effects on predicted activation entropies in the benchmark study.

This study focuses on elucidating the mechanism of backbiting and β-scission reactions in self-initiated polymerization of methyl acrylate using G4(MP2)-6X, DFT, and MP2 methods. We studied four types of intramolecular hydrogen transfer, 1:3, 1:5, 1:7, and 1:9 backbiting, as shown in Figure 2. Each of the secondary live polymer chains undergoing backbiting is self-initiated with a DMR or a MMR. The effect of the type of initiating monoradical on the various mechanisms and kinetics is investigated. The length of secondary live polymer chains, SPRs, is varied from 3 to 6 monomers, and the effect of chain length on energy barrier and rate constants of backbiting and β-scission reactions is studied. The ^{13}C-NMR and ^{1}H-NMR chemical shifts of species generated from the backbiting and β-scission reactions are computed and compared with those obtained from laboratory experiments.

Computational Method

The G4(MP2)-6X calculations are performed with Gaussian 09[61] to take advantage of the parallel algorithm of open-shell

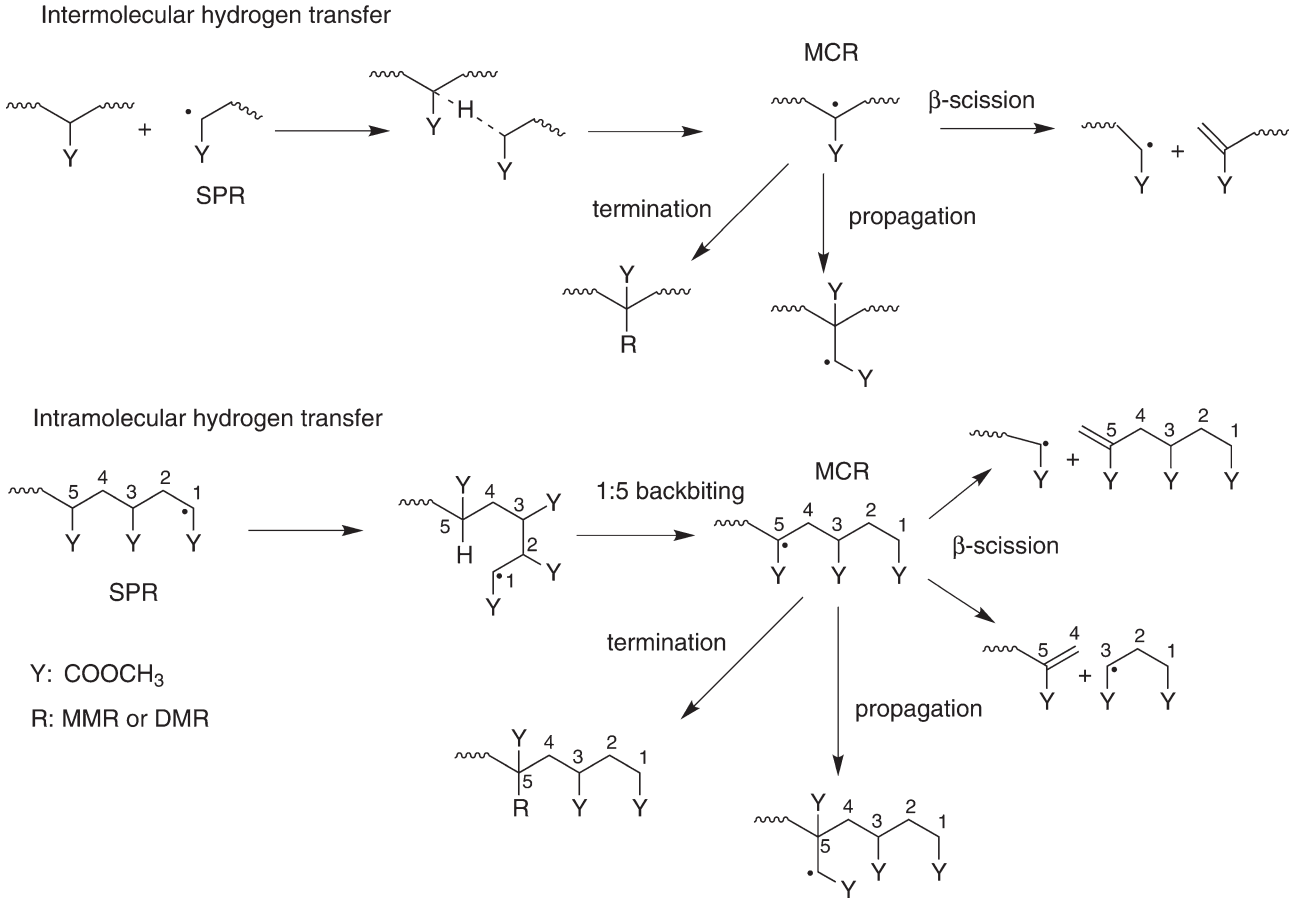

Figure 1. Intermolecular and intramolecular hydrogen transfer reactions in spontaneous thermal homopolymerization of methyl acrylate.

CCSD(T) calculation. 1D-HR and RRHO approximations are used and compared in the benchmark study. The rotational potential is scanned with 12 sampling points, which has been found to be adequate to capture the features of the energy profiles.[36,37] All other calculations are carried out using GAMESS.[62] The geometries of reactants, products, and the transition-state structures from different reaction mechanisms are optimized with three different functionals, B3LYP, M06-2X, and PBE0, with the 6-31G* basis set and restricted-open-shell Hartree-Fock (ROHF) wave functions. Previous studies[63,64] of radical propagation reactions revealed that the application of unrestricted-open-shell Hartree-Fock (UHF) wavefunctions suffers from the problem of spin contamination, and ROHF wavefunctions improve the results. This rendered us to apply ROHF over UHF in current study. In addition, it has been reported that the choice of UHF or ROHF has little influence on molecular structures and energetics predicted using high-level methods such as coupled cluster calculations.[65] It is important to note that UHF is used in G4(MP2)-6X calculations. Hessian calculations were carried out to determine the vibrational frequencies of reactants and products and transition states. The geometries with zero imaginary frequencies are reactants and products, with one imaginary frequency for a transition state. Vibrational frequency scaling factors have been applied.[47] As the tunneling effect becomes important for hydrogen transfer reaction,[66] we apply the Eckart tunneling correction[67] to compute the rate constants for hydrogen transfer reactions based on transition-state theory.[68] The Wigner tunneling correction method[69] is used for β-scission reactions. Detailed formulas for Eckart and Wigner corrections can be found in our previous work[70] and Supporting Information. The rate constant at a temperature T, $k(T)$, is then calculated using

$$k(T)=\kappa(c^{\circ})^{1-m}\frac{k_B T}{h}\exp\frac{\Delta S^{\neq}}{R}\exp\frac{-\Delta H^{\neq}}{RT} \quad (3)$$

in which κ is the tunneling correction, c° is the inverse of the reference volume assumed in the calculation of translational partition function, m is the molecularity of the reaction, h is Planck constant, k_B is the Boltzmann constant, R is the ideal gas constant, $\Delta S^{\neq}$ is the entropy of activation, and $\Delta H^{\neq}$ is the enthalpy of activation.

The absolute isotropic shielding for the carbon nuclei is calculated using the individual gauge for localized orbitals procedure[71,72] in the ORCA software package[73] with the B3LYP/6-31G* functional/basis set. Tetramethylsilane is chosen as the NMR reference. The target chemical shifts are computed by subtracting the reference absolute isotropic shielding from the target.

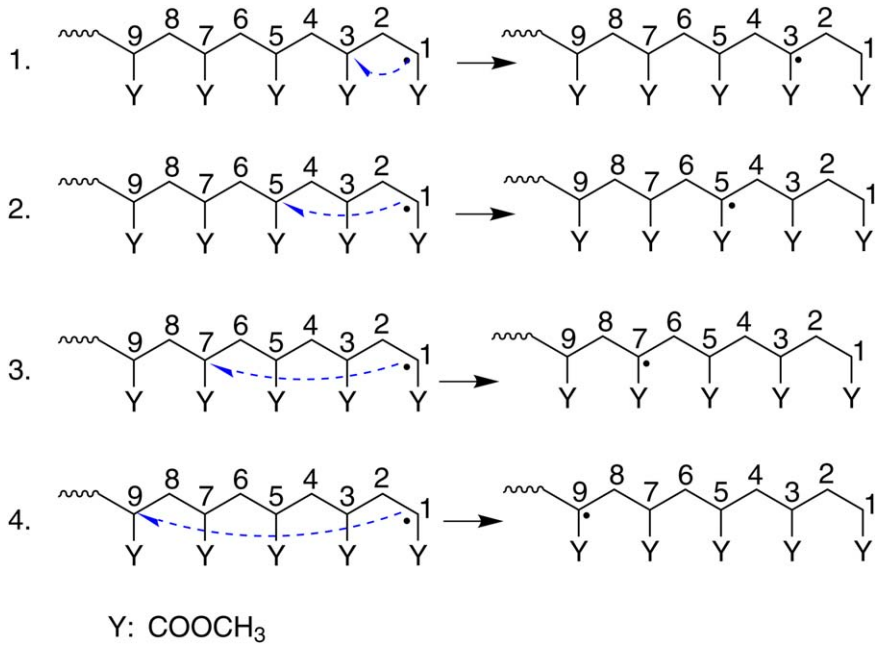

Figure 2. Various intramolecular hydrogen transfer reactions of a secondary propagating radical (SPR) in spontaneous thermal polymerization of methyl acrylates. 1, 1:3 Backbiting; 2, 1:5 Backbiting; 3, 1:7 Backbiting; 4, 1:9 Backbiting. [Color figure can be viewed in the online issue, which is available at wileyonlinelibrary.com.]

Results and Discussions

Benchmark study of the 1:5 backbiting reaction

Composite Method versus DFT and MP2. The 1:5 backbiting reaction of a MMR-initiated SPR with three monomer units (3MSPR) shown in Figure 3a is chosen as the representative reaction for the benchmark comparison of this composite method versus DFT and MP2. Table 1 presents the electronic energy barriers calculated with G4(MP2)-6X, B3LYP, M06-2X, PBE0, and MP2 with various basis sets. It indicates that energy barriers calculated using B3LYP and M06-2X are comparable to that calculated using G4(MP2)-6X, and the size of the basis set does not have a significant effect on the energy barrier. B3LYP underestimated the barrier, and M06-2X overestimated the barrier relative to that of G4(MP2)-6X. This trend is opposite to that observed for radical propagation of methyl acrylate, where B3LYP predicts a larger barrier than M06-2X.[41] As B3LYP and M06-2X performed equally well for backbiting reactions, these functionals are used in our further studies with 6-31G* basis set. Although PBE0 predictions deviate the most from those of G4(MP2)-6X, we still use this functional to understand its performance for large polymers.

HO versus 1D-HR. Figure 3b shows the internal rotations about all the single bonds in the transition-state structure for the 1:5 backbiting reaction of 3MSPR. It should be noted that the sigma bonds that form the six-membered ring structure in the transition state cannot rotate. We treated 10 low frequency modes as HRs in the initial propagating radical and the transition state. The activation entropy and frequency factor calculated using the HO approximation are −10.0 J/mol/K and 5.11 $\times$ 10^{12}, and using HR approximation are −3.0 J/mol/K and 1.18 $\times$ 10^{13}. These calculated frequency factors are similar to the values reported by Yu and Broadbelt[42] for methyl acrylate and *n*-butyl acrylate using HR approximations. It can be seen that difference between HO and HR approximations is about a factor of 2. This show that the less expensive yet accurate HO approximation can be used for all practical purposes in calculating the rate constants of various reactions in thermal polymerization of alkyl acrylates.

Quantum Chemistry Comparison with Laboratory Experiments. For free-radical polymerization of *n*BA, macroscopic mechanistic models have been used to provide estimates of the preexponential factor and activation energy: (4.8–7.4) $\times$ 10^7 s^{-1} and (31.7 –32.7) kJ/mol for backbiting reaction, and (1.49 $\pm$ 0.28) $\times$ 10^9 s^{-1} and (63.9 $\pm$ 0.9) kJ/mol for β-scission reaction.[27,29,46] The accuracy of these estimates depends on the reliability of polymer sample measurements and the reaction mechanisms assumed. Such an "experimental" value (estimated from polymer sample measurements) for the rate constant of the 1:5 backbiting reaction of MA has not been reported in the open literature. On the other hand, it has been suggested that the 1:5 backbiting reaction rate constant of MA has a value close to that of *n*BA.[11,42] In view of these, it is worthwhile to compare Arrhenius parameter values of the 1:5 backbiting reaction of MA obtained using quantum chemistry methods to experimental values of *n*BA.[26,29] Both G4(MP2)-6X and DFT-calculated values of the activation energy of the MA reaction are about 28 kJ/mol higher than the experimental value of the same parameter for *n*BA, whereas the frequency factor estimated with the HR approximation ($\sim$$10^{12}$ s^{-1}) is

Table 1. Electronic energy barriers in kJ/mol estimated with different methods.

B3LYP	E_0	M06-2X	E_0	PBE0	E_0	MP2	E_0
6-31G*	74.6	6-31G*	86.3	6-31G*	68.5	6-31G*	72.7
6-311G*	75.8	6-311G*	88.8	6-311G*	69.6	6-311G*	72.3
6-311G**	72.4	6-311G**	86.2	6-311G**	66.0	6-311G**	64.9
6-31+G*	72.8	6-31+G*	84.4	6-31+G*	67.1	6-31+G*	70.3
6-31+G**	70.7	6-31+G**	83.1	6-31+G**	64.9	6-31+G**	65.7
6-31+G(2*df,p*)	71.1	6-31+G(2*df,p*)	84.2	6-31+G(2*df,p*)	64.6	6-31+G(2*df,p*)	62.7
G4(MP2)-6X				80.3			

about five orders of magnitude higher than the experimental value of *n*BA.[26,29] However, in terms of reaction rate constant, these theoretical and experimental values show reasonable agreement. Furthermore, these findings are in agreement with those reported by Yu and Broadbelt[42] and Cuccato et al.[44,45] It appears that even the use of the state-of-art electronic structure calculation method (G4(MP2)-6X) and a sophisticated entropy calculation approach (HR approximation) does not result in eliminating the discrepancy between the theoretical and experimentally deduced values of the activation energy and frequency factor. The fact that DFT-estimated rate constant agrees with the experimental value is attributed to the large error cancellation in electronic structure calculation and entropy calculation when studying liquid-phase reactions in gas-phase.[74] However, the origin of such large error cancellation is not clear. Therefore, while it is legitimate to perform first-principles calculations in gas phase for reactions actually occurring in liquid phase (given the good performance of DFT in predicting rate constants), we suggest that further computational studies using a more realistic model (including solvation model) and more accurate method for entropy calculations in liquid phase are still required. Also, the refinement of the mechanistic reaction models for macroscopic modeling is of great importance.

Backbiting reactions of DMR-initiated live polymer chains

We studied the 1:3 and 1:5 backbiting reactions for DMR-initiated SPRs with four monomer units (4DSPR), 1:3, 1:5, and 1:7 backbiting reactions for SPRs with five monomer units (5DSPR), and 1:3, 1:5, 1:7, 1:9 backbiting reactions for SPRs with six monomer units (6DSPR), as shown in Figure 4. The transfer of a hydrogen atom (H_t) from the midchain carbon atoms C3, C5, C7, and C9 to the terminal carbon (C1) correspond to 1:3, 1:5, 1:7, 1:9 backbiting mechanisms. The potential energy surface is explored by choosing r_1(C1-H_t) and r_2(C*n*-H_t) for 1:*n* backbiting (n = 3,5,7,9) as reaction coordinates. Table 2 gives the values of r_1, r_2, and the angle between them in the transition-state geometry for various backbiting mechanisms optimized using B3LYP, PBE0, and M06-2X. Our results indicate that the difference in bond length is within 0.05 Å and the variation in bond angle is within 5° for the three functionals. This suggests that the geometry optimization is not affected appreciably by the change in density functional. The

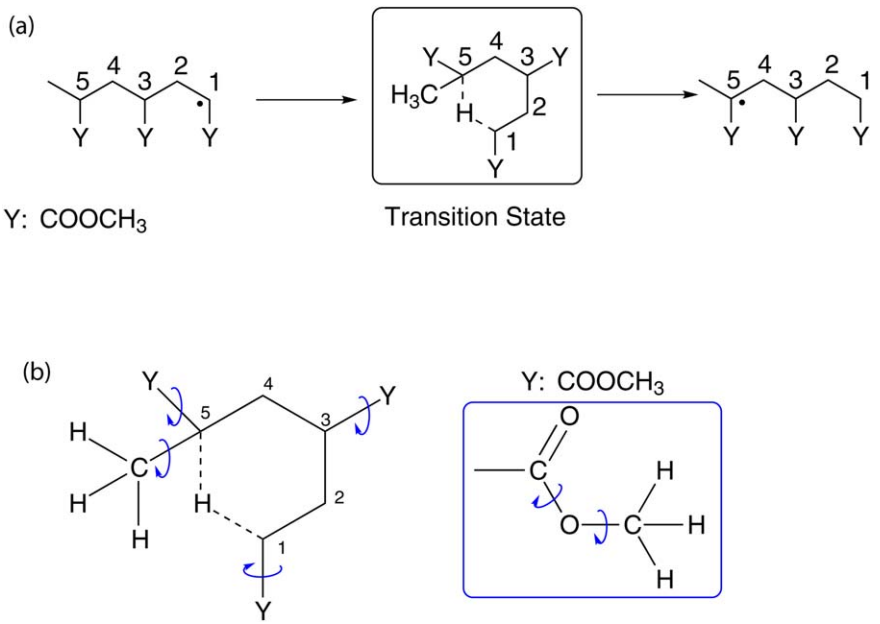

Figure 3. a) The 1:5 backbiting reaction of 3MSPR for benchmark study. b) Rotational axes of hindered rotors in 1D-HR approximation. [Color figure can be viewed in the online issue, which is available at wileyonlinelibrary.com.]

Table 2. Optimized geometry of transition state for various backbiting mechanisms using B3LYP/6–31G*, M06–2X/6–31G*, and PBE0/6–31G*.

		B3LYP			M06-2X			PBE0		
SPR	Scheme	r_1 (Å)	r_2 (Å)	∠CHC	r_1 (Å)	r_2 (Å)	∠CHC	r_1 (Å)	r_2 (Å)	∠CHC
4DSPR	1:3	1.41	1.41	103.56	1.42	1.39	103.26	1.40	1.4	103.22
4DSPR	1:5	1.38	1.32	151.97	1.38	1.31	150.46	1.38	1.31	151.33
5DSPR	1:3	1.41	1.41	103.31	1.41	1.38	102.94	1.40	1.39	103.18
5DSPR	1:5	1.37	1.35	156.59	1.38	1.34	153.31	1.36	1.34	156.69
5DSPR	1:7	1.34	1.37	171.89	1.32	1.35	178.39	1.33	1.36	171.86
6DSPR	1:3	1.42	1.41	103.16	1.41	1.38	102.86	1.41	1.38	102.77
6DSPR	1:5	1.34	1.40	154.42	1.30	1.36	156.82	1.37	1.31	155.60
6DSPR	1:7	1.37	1.35	165.42	1.37	1.35	165.42	1.37	1.35	165.42
6DSRP	1:9	1.41	1.37	167.44	1.40	1.36	167.07	1.40	1.36	166.88
3MSPR	1:3	1.42	1.41	103.37	1.42	1.39	103.08	1.41	1.39	103.12
3MSPR	1:5	1.37	1.33	152.22	1.37	1.31	149.72	1.37	1.32	150.82
4MSPR	1:3	1.41	1.40	103.00	1.41	1.38	102.82	1.40	1.39	102.62
4MSPR	1:5	1.37	1.35	155.40	1.38	1.33	154.63	1.35	1.34	155.25
4MSPR	1:7	1.35	1.32	172.62	1.38	1.35	166.07	1.35	1.32	172.70
5MSPR	1:3	1.41	1.39	104.31	1.41	1.38	103.18	1.41	1.39	103.25
5MSPR	1:5	1.31	1.37	156.42	1.34	1.40	154.86	1.31	1.37	156.00
5MSPR	1:7	1.37	1.35	165.37	1.37	1.36	166.04	1.37	1.36	164.48
5MSPR	1:9	1.41	1.38	168.17	1.36	1.40	167.01	1.40	1.36	167.88

calculated activation energies and rate constants are given in Table 3. Table 4 presents the kinetic constants obtained with 6-31G** basis set. These results indicate that the estimated thermodynamics parameters are not affected strongly by the 6-31G* and 6-31G** basis sets.

Tables 3 and 4 indicate that the 1:5 backbiting reaction is generally more energetically favored than 1:3 and 1:9 backbiting reactions. This agrees with previous work on backbiting reactions of styrene, vinyl chloride, and ethylene.[75–77] The transition-state structures of backbiting reactions of 6DSPR using B3LYP/6-31G* are shown in Figure 5. The six-membered ring transition-state structure of the 1:5 mechanism shown in Figure 5 has five carbons with bond angles of 101.2°, 114.2°, 111.8°, 114.7°, and 99.7°. The four-membered ring transition state structure of the 1:3 mechanism has three carbon atoms with bond angles of 93.0°, 81.7°, and 81.6°. The bond angles of the carbon atoms involved in the transition-state structure of the 1:7 and 1:9 mechanisms are between 105° and 119°. It appears that the bond angles in the transition-state structure of the 1:5 backbiting are close to the angles of sp^3 hybridization (bond angle ≈109.5°). The smaller bond angles in the 1:3 transition-state structure indicate a more strained structure with a higher energy. The transition states of 1:7 and 1:9 backbiting mechanisms appear to be less strained, which can be attributed to the ability of the longer chains to rearrange and distribute the strain. However, the internal rearrangement to achieve the desired orientation for hydrogen transfer is speculated to be the cause for the increase in the energy barrier. All three levels of theory predict that the energy barrier for 1:5 is comparable to that of the 1:7 backbiting mechanism for 6DSPR, with 1:3 and 1:9 considerably higher. The energy barrier of the 1:5 mechanism is lower than that of 1:7 in 5SPDR. This suggests that the chain length may have an influence on the type of backbiting mechanism that is most likely to occur; the longer 6DSPR chain allows the radical center to achieve the desired orientation by coiling itself to undergo 1:7 hydrogen transfer reaction. This agrees with experimental reports that have shown the presence of remote backbiting in thermal polymerization of alkyl acrylates using electron paramagnetic resonance spectroscopy.[21]

Backbiting reactions of MMR-initiated live polymer chains

Backbiting reactions of MMR-initiated SPRs with a chain length of three to five monomer units are explored using B3LYP, PBE0, and M06-2X/6-31G* (Fig. 4). The 1:3 and 1:5 backbiting mechanisms are investigated for live polymer chains with three monomer units (3MSPR), the 1:3, 1:5, 1:7 backbiting mechanisms for live polymer chains with four monomer units (4MSPR), and the 1:3, 1:5, 1:7, 1:9 backbiting mechanisms for live polymer chains with five monomer units (5MSPR). Table 2 gives r_1, r_2, and bond angles of the transition state structures. The results again indicate that the geometries of the transition-state structures calculated using different density functionals M06-2X/6-31G*, B3LYP/6-31G*, and PBE0/6-31G* are similar. The highest activation energy was obtained using M06-2X/6-31G*, and the lowest using PBE0/6-31G*. Also, the use of a different basis set, 6-31G**, showed a similar finding: the geometries of the identified transition-state structures are similar, and the calculated activation energies have the same trend (higher energies with M06/6-31G** and lower energies with PBE0/6-31G** relative to B3LYP/6-31G**). The 1:5 and 1:7 backbiting mechanisms are more kinetically favored than the 1:3 and 1:9 backbiting ones. The 1:5 mechanism has a lower energy barrier than the 1:7 one for 5MSPRs, which is comparable to our earlier findings for 5DSPRs. These results indicate that the type of initiating species does not influence the kinetics of backbiting reactions for live chains with the same polymer chain length (e.g., 5DSPR and 5MPR). The Mulliken charge analysis indicates little variation in electron density of

Table 3. Activation energy (E_a), activation free energy ($\Delta G^{\neq}_{298K}$) in kJ/mol; Eckart tunneling correction (κ_E); frequency factor (A), and rate constant (k) in s^{-1} at 298 K for backbiting reactions using B3LYP/6-31G*, M06-2X/6-31G*, and PBE0/6-31G*.

		B3LYP					M06-2X					PBE0				
SPR	Scheme	E_a	$\Delta G^{\neq}_{298K}$	lnA	κ_E	k	E_a	$\Delta G^{\neq}_{298K}$	lnA	κ_E	k	E_a	$\Delta G^{\neq}_{298K}$	lnA	κ_E	k
4DSPR	1:3	155.64	151.75	31.03	2.61E5	4.19E-9	163.78	167.32	28.03	9.56E4	2.87E-12	149.97	152.82	28.31	2.11E5	2.21E-9
4DSPR	1:5	59.18	67.58	26.07	4.29E1	3.85E2	70.53	70.52	29.46	2.69E1	7.40E1	53.34	53.90	29.23	2.28E1	5.10E4
5DSPR	1:3	163.40	161.99	30.03	3.08E5	7.97E-11	165.64	165.29	29.60	5.23E4	3.58E-12	150.35	156.45	27.00	1.12E5	2.70E-10
5DSPR	1:5	58.04	69.10	25.00	6.43E1	3.13E2	51.81	57.78	27.05	1.70E2	7.96E4	49.27	69.16	21.43	1.03E2	4.88E2
5DSPR	1:7	62.13	68.53	26.88	9.72E1	5.94E2	67.13	73.21	27.00	2.54E1	2.36E1	54.55	66.86	24.49	4.63E1	5.56E2
6DSPR	1:3	142.13	163.09	21.00	1.27E5	2.11E-11	155.95	154.31	30.12	8.42E4	4.82E-10	140.23	123.01	36.40	6.84E4	1.19E-4
6DSPR	1:5	79.31	78.51	29.78	1.36E2	1.49E1	83.84	89.98	26.98	1.59E1	1.70E-2	70.62	73.71	28.21	2.83E1	2.15E1
6DSPR	1:7	78.41	75.10	30.79	5.09E2	2.21E2	78.87	71.95	32.25	4.61E1	7.08E1	67.83	74.82	26.64	1.02E2	4.92E1
6DSPR	1:9	105.44	111.02	27.20	1.40E3	3.07E-4	117.13	111.79	31.61	3.21E2	5.18E-5	96.77	100.95	27.77	4.38E2	5.61E-3
3MSPR	1:3	153.95	159.24	27.32	2.48E5	1.95E-10	162.95	162.77	29.53	6.84E4	1.29E-11	146.92	151.40	27.65	1.41E5	2.61E-9
3MSPR	1:5	63.50	61.21	30.38	4.19E1	4.91E3	74.14	70.40	30.97	3.81E1	1.10E2	56.26	53.08	30.74	2.62E1	8.17E4
4MSPR	1:3	157.75	161.14	28.09	2.12E5	7.70E-11	162.54	157.33	31.56	5.20E4	8.81E-11	149.73	154.97	27.34	8.36E4	3.66E-10
4MSPR	1:5	50.08	56.42	26.90	5.12E1	4.15E4	60.40	58.59	30.19	3.19E1	1.07E4	42.60	52.94	25.29	2.76E1	9.09E4
4MSPR	1:7	71.68	73.79	28.61	2.81E1	2.07E1	70.82	73.92	28.21	8.17E1	5.68E1	64.87	67.66	28.33	2.76E1	2.40E2
5MSPR	1:3	141.80	148.70	26.67	2.38E4	1.31E-9	142.70	144.75	28.63	1.58E4	4.28E-9	132.93	140.90	26.24	4.58E4	5.87E-8
5MSPR	1:5	56.96	65.17	26.15	2.40E1	5.71E2	60.85	63.18	28.52	5.86E1	3.10E3	48.86	50.57	28.77	2.59E1	2.22E5
5MSPR	1:7	78.94	83.75	27.51	5.17E1	6.81E-1	79.57	80.41	29.12	5.06E1	2.57	67.78	69.88	28.61	7.23E1	2.56E2
5MSPR	1:9	105.19	112.90	26.34	4.29E2	4.41E-5	104.15	106.65	28.45	1.75E2	2.25E-4	92.75	101.10	26.09	4.75E2	5.73E-3

Table 4. Activation energy (E_a), activation free energy ($\Delta G^{\neq}_{298K}$) in kJ/mol; Eckart tunneling correction (κ_E); frequency factor (A), and rate constant (k) in s^{-1} at 298 K for backbiting reactions using B3LYP/6-31G**, M06-2X/6-31G**, and PBE0/6-31G**.

		B3LYP					M06-2X					PBE0				
SPR	Scheme	E_a	$\Delta G^{\neq}_{298K}$	lnA	κ_E	k	E_a	$\Delta G^{\neq}_{298K}$	lnA	κ_E	k	E_a	$\Delta G^{\neq}_{298K}$	lnA	κ_E	k
4DSPR	1:3	152.40	154.20	28.73	2.52E5	1.51E-9	160.60	165.24	27.59	6.57E4	4.58E-12	145.87	149.04	28.18	1.18E5	5.66E-9
4DSPR	1:5	57.25	65.43	26.16	3.08E1	6.60E2	69.27	70.41	29.00	2.53E1	7.24E1	51.50	52.96	28.87	1.76E1	5.76E4
5DSPR	1:3	159.28	158.07	29.95	2.36E5	2.97E-10	162.97	163.19	29.37	3.35E4	5.32E-12	145.89	152.52	26.79	6.12E4	7.23E-10
5DSPR	1:5	55.02	65.08	25.40	5.31E1	1.31E3	49.74	56.44	26.76	4.05E1	3.25E4	46.47	60.35	23.86	2.85E1	4.72E3
5DSPR	1:7	59.41	65.96	26.81	6.09E1	1.05E3	65.68	72.41	26.74	2.24E1	2.86E1	52.12	61.70	25.59	2.88E1	2.77E3
6DSPR	1:3	138.82	149.42	25.18	8.04E4	3.32E-9	152.59	150.89	30.14	3.44E4	7.78E-10	135.95	119.55	36.07	2.54E4	1.79E-4
6DSPR	1:5	76.92	76.54	29.61	1.13E2	2.73E1	82.54	83.70	28.99	1.65E1	2.22E-1	68.65	66.26	30.42	2.31E1	3.53E2
6DSPR	1:7	75.43	76.79	28.91	8.43E1	1.85E1	77.97	72.54	31.65	2.55E1	3.09E1	65.14	66.98	28.72	3.70E1	4.24E2
6DSPR	1:9	103.01	110.12	26.59	9.73E2	3.08E-4	116.26	107.52	32.98	3.15E2	2.84E-4	93.86	97.12	28.14	3.14E2	1.88E-2
3MSPR	1:3	149.77	154.15	27.69	1.88E5	1.15E-9	158.34	153.90	31.25	5.02E4	3.40E-10	142.62	146.50	27.89	8.24E4	1.10E-8
3MSPR	1:5	61.10	58.37	30.56	3.68E1	1.36E4	73.21	70.10	30.71	3.12E1	1.01E2	54.41	53.63	29.77	2.16E1	5.38E4
4MSPR	1:3	153.43	156.59	28.18	1.53E5	3.49E-10	160.06	155.81	31.17	3.49E4	1.09E-10	145.43	150.71	27.33	5.62E4	1.38E-9
4MSPR	1:5	46.97	52.32	27.30	4.16E1	1.75E5	57.55	51.03	32.09	3.50E1	2.49E5	39.71	47.42	26.35	2.31E1	7.03E5
4MSPR	1:7	69.45	71.58	28.60	2.38E1	4.26E1	69.90	71.10	28.98	7.03E1	1.53E2	63.36	68.10	27.54	2.24E1	1.63E2
5MSPR	1:3	138.32	144.93	26.79	6.01E4	1.51E-8	139.21	138.70	29.66	1.44E4	4.48E-8	129.32	137.66	26.09	2.87E4	1.36E-7
5MSPR	1:5	54.68	61.09	26.87	2.52E1	3.10E3	59.14	53.55	31.71	5.92E1	1.52E5	46.98	49.16	28.58	1.81E1	2.74E5
5MSPR	1:7	75.45	81.25	27.12	8.03E1	2.91	78.84	74.60	31.17	5.56E1	2.94E1	65.53	68.01	28.46	6.08E1	4.60E2
5MSPR	1:9	101.74	109.42	26.36	8.94E2	3.75E-4	101.89	96.56	31.61	2.54E2	1.90E-2	90.53	101.24	25.14	3.52E2	4.00E-3

International Journal of QUANTUM CHEMISTRY

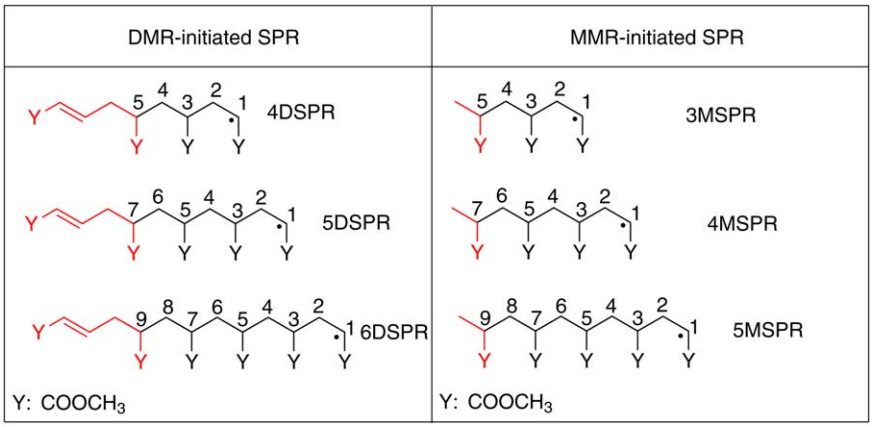

Figure 4. Structures of SPRs studied in this work. The initiator-end is colored in red. [Color figure can be viewed in the online issue, which is available at wileyonlinelibrary.com.]

the transfer center (tertiary carbon) with the type of initiating groups (DMR and MMR).

Effects of side chains

Yu and Broadbelt[42] studied the 1:5 backbiting of MA and *n*BA with a four-monomer polymer chain. Cuccato et al.[44] studied four types of backbiting reactions of *n*BA with a simplified molecular model in which the side chains of monomer units were replaced with hydrogen atoms except those (e.g., C1 and C5 for 1:5 backbiting reaction) directly participate in the hydrogen transfer. We compare transition-state structures and kinetic constants obtained using full-atomic models of Yu and Broadbelt and ours presented in this article to those obtained using the simplified model of Cuccato et al. These studies indicate that the side chains have no significant impact on either the located transition-state geometry or rate coefficients for the 1:5 backbiting reaction: the differences in r_1 and r_2 values are within 0.05 Å, the activation energies are similar [53 kJ/mol (Yu and Broadbelt), 50 kJ/mol (this work for 4MSPR), and 55 kJ/mol (Cuccato et al.)], and the rate constants are of the same order of magnitude. However, the rate constants for 1:7 and 1:9 backbiting reactions obtained using the complete molecular model are 3–4 orders of magnitude higher than those obtained using the simplified model.[44] This is due to larger frequency factors predicted by the complete molecular model that accounts for the side chains. It is probable that the substitution of side chains with hydrogen atoms in the simplified model underestimates the entropy change for those long-range hydrogen transfer reactions that involve a large change of polymer conformations. This is the common trade-off between model simplicity and model-prediction accuracy. In addition, the comparable rate constant values reported in this work, by Yu and Broadbelt and by Cuccato et al. indicate that the type of initiating radical [self-initiation (DMR and MMR) vs. external (peroxide/azonitrile)] does not influence the backbiting mechanisms.

β-scission reactions of MCRs

The two cleavage mechanisms, R-side β-scission [which produces a macromonomer (dead polymer chain) including one of the two initiating groups] and L-side β-scission (which produces a SPR including one of the two initiating groups), are shown in Figure 6. The β-scission reactions are explored using the two reaction coordinates: r_s is the bond length of the σ bond (one carbon away from the radical site) to be broken, and r_d is the bond length of the double bond to be formed. Table 5 gives the values of r_s, r_d, and the angle between the σ bond and the double bond in the transition-state structures. The computational results indicate that the four-monomer DMR-initiated MCRs (4DMCR^5) and three-monomer MMR-initiated MCRs (3MMCR^5) can only undergo R-side β-scission, as the L-side β-scission produces an allene that is energetically unstable. This suggests that the R-side β-scission is dominant for short-chain MCRs. Figure 7 shows the transitions states of β-scission reactions of the six-monomer DMR-initiated MCRs (6DMCR^5). The molecular geometries are insensitive to the functional, which agrees with our previous findings for

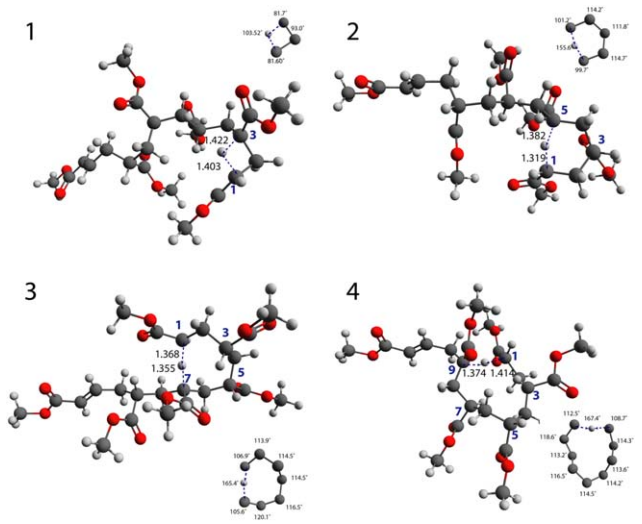

Figure 5. Transition states of backbiting reactions of 6DSPR. **1**, transition state of 1:3 backbiting; **2**, transition state of 1:5 backbiting; **3**, transition state of 1:7 backbiting; **4**, transition state of 1:9 backbiting. All interatomic lengths are in Å. The bond angles in the ring structure of the transition state are labeled. [Color figure can be viewed in the online issue, which is available at wileyonlinelibrary.com.]

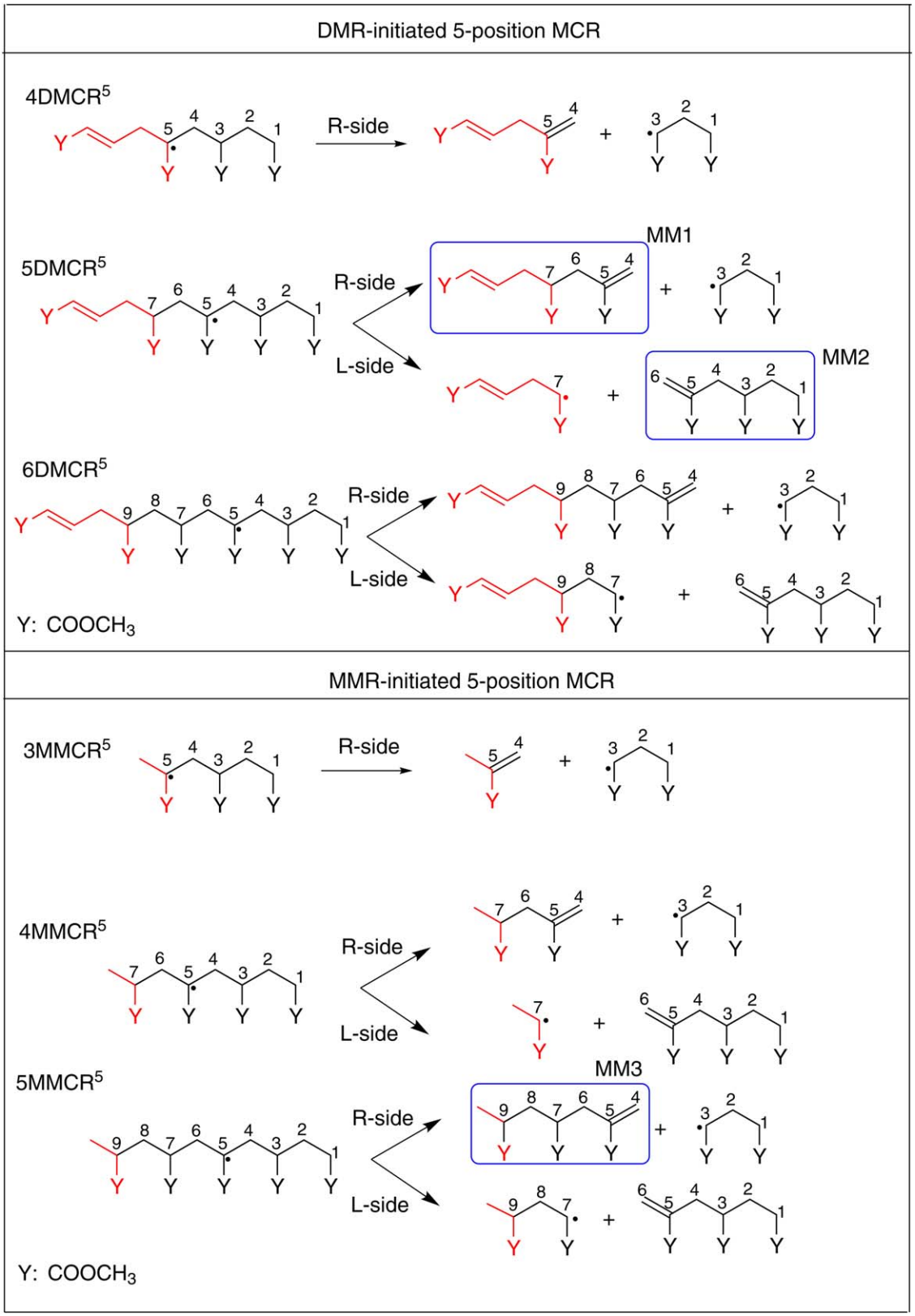

Figure 6. β-scission reactions of DMR- and MMR-initiated MCRs. The initiator-end is colored red. [Color figure can be viewed in the online issue, which is available at wileyonlinelibrary.com.]

backbiting reactions. As given in Tables 6 and 7, both M06-2X and PBE0 predict higher energy barriers than B3LYP consistently. It has been reported[78] that B3LYP (20% HF exchange) gives a repulsive potential for van der Waals complexes, whereas PBE0 (25% HF exchange) gives an attractive potential with a shallow well, and M06-2X (54% HF exchange) produces

a deeper well. This suggests that the higher energy barriers calculated using M06-2X and PBE0 are likely due to the intramolecular noncovalent attractive interactions captured by the HF exchange as the fragments move away from each other in the cleavage mechanisms. Using the geometries optimized with M06-2X (54% HF exchange) for the β-scission reaction of 3MMCR,[5] we further calculate the energy barriers with M06-L (no HF exchange) and M06 (27% HF exchange). The values of energy barriers obtained with M06-L/6-31G*, M06/6-31G*, and M06-2X/6-31G* are, respectively, 108.7, 119.5, and 127.4 kJ/mol, which indicate that a functional with a larger amount of exact exchange tends to predict a higher energy barrier. The use of different functionals indicates that the R-side and L-side β-scission have comparable energy barriers. The length of the live polymer chain does not affect the energy barrier significantly. This can be attributed to the bond cleavage and formation in β-scission reactions occurring locally, with little change in the overall conformation of the polymer chain. For example, in the R-side β-scission of 6DMCR, the major change is the increase of r_s from 1.59 Å in reactant to 2.27 Å in transition state, the decrease of r_d from 1.50 Å to 1.38 Å, and the slight reduction of the angle from 115° to 112°, while no significant change for the geometries outside the reaction center is found (see the Supporting Information for a detailed comparison). β-Scission rate constants calculated using B3LYP/6-31G* are in the range of 10^{-4} s^{-1} and agree reasonably well with previous experimental and theoretical work.[26,45] We found that the rate constants of some type of β-scission reactions are 1–2 orders of magnitude higher or lower than 10^{-4}, which is probably due to the dedicated intermolecular interactions between two fragments after cleavage. This may be a result of overestimation of the effect of the intermolecular interactions in gas-phase calculations. Future research involving the use of a solvation model may help identify the origin of restarted/facilitated β-scission reactions.

Calculated versus experimental NMR spectra

The ^{13}C-NMR chemical shifts of species generated from backbiting and β-scission reactions are calculated. Figure 8 depicts the calculated molecular structures and chemical shifts of polymer chains that are formed from the backbiting reactions of 5DSPR and 4MSPR. The linear polymer chain generated from the termination of 5DSPR via MMR is labeled as 5DSPR-MMR. We consider three possible branched polymers, resulting from the termination between 3-position MCR and MMR (5DMCR^3-MMR), 5-position MCR and MMR (5DMCR^5-MMR), and 7-position MCR and MMR (5DMCR^7-MMR). Similarly, the polymer chains incorporating 4MSPR are named as 4MSPR-MMR, 4MMCR^3-MMR, 4MMCR^5-MMR, and 4MMCR^7-MMR. We also calculate the ^{13}C-chemical shifts of three different macromonomers (MM1, MM2, and MM3), as shown in Figure 6. MM1 and MM3 are from the R-side β-scission and MM2 is from L-side β-scission. Figure 9 shows calculated ^{1}H NMR spectra of the macromonomers, and Figure 10 presents calculated ^{13}C NMR spectra.

The calculated chemical shifts of different types of carbon nuclei are summarized and are compared to experimental values taken from Quan et al.[4] in Table 8. As given in Table 8, the calculated and experimental chemical shifts are comparable for various functional groups on the polymer backbone, side chain, and branches. This indicates that B3LYP/6-31G* is a cost-effective method to predict the NMR chemical shifts of polymer chains of methyl acrylates. Our findings agree with previous studies[79,80] that relatively simple basis sets (e.g., 6-31G*) and hybrid functionals (e.g., WP04 and B3LYP) can predict the chemical shifts with reasonable accuracy. The range of calculated chemical shifts with B3LYP/6-31G* is slightly larger than that of experiments. This may indicate that we computationally explored more types of polymer chains than those produced in the polymerization experiments. Our results indicate that the chemical shifts of the quarternary carbon (C_q), methoxy (OCH_3), and unsaturated (C=C) end group are unaffected by the position of the branch (Fig. 8). Furthermore, the ^{13}C shift of end group methyl from MMR initiating radicals vary from 13.0–21.3 ppm depending on the position of the branch.

Previous studies[4,22] suggested that the β-scission reaction is mainly responsible for the presence of terminal vinyl carbons in the polymer chains obtained from high-temperature polymerization. Our calculated ^{1}H NMR spectra of macromonomers are consistent with reported experimental ^{1}H NMR

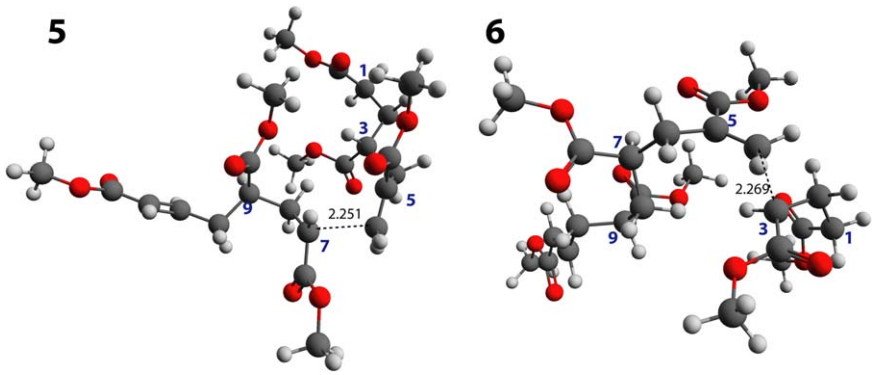

Figure 7. Transition states of β-scission reactions from 6DMCR5. **5**, transition state of L-side β-scission; **6**, transition state of R-side β-scission. [Color figure can be viewed in the online issue, which is available at wileyonlinelibrary.com.]

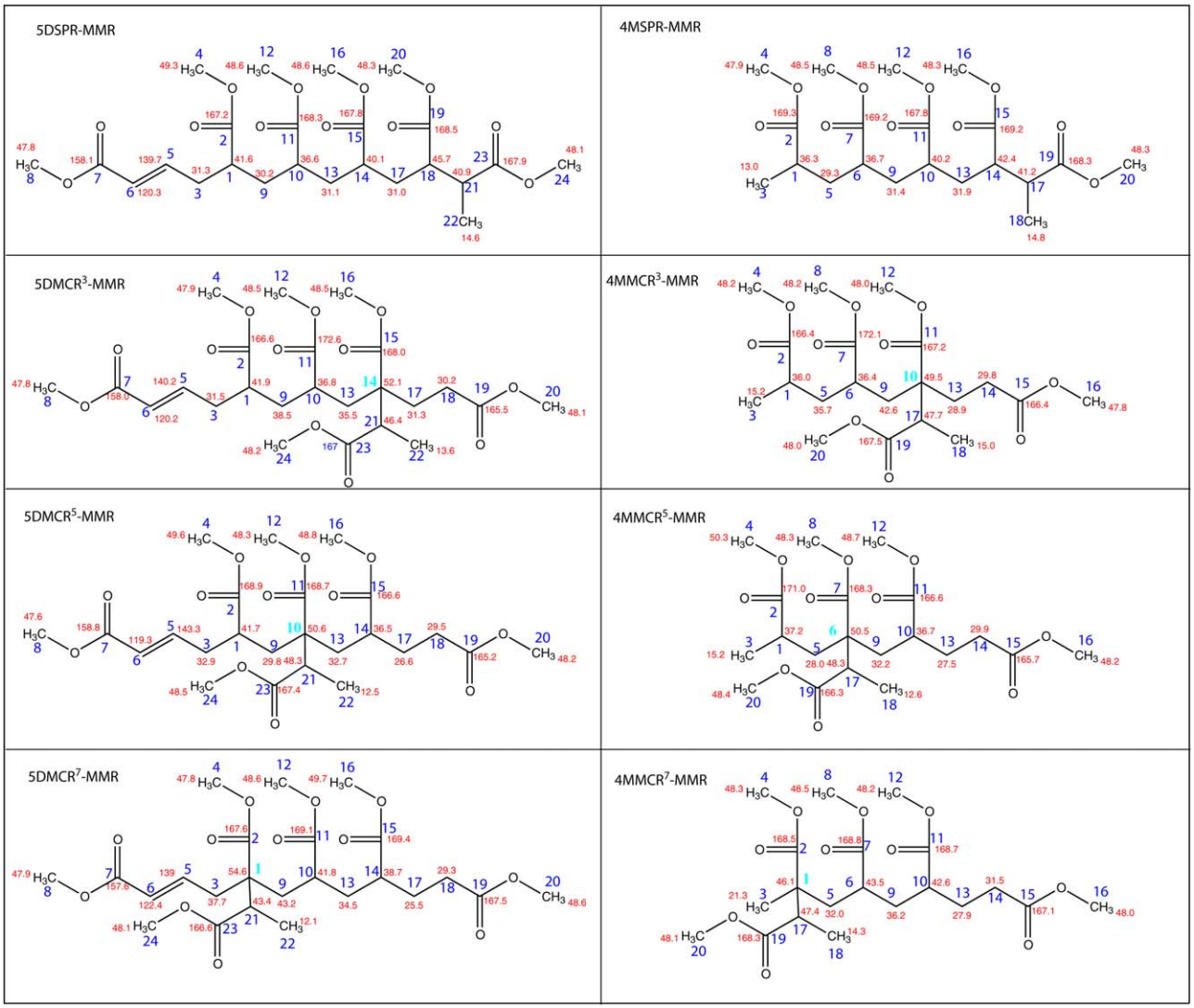

Figure 8. Calculated chemical shifts of C nucleus in linear polymers and branched polymers of methyl acrylate. [Color figure can be viewed in the online issue, which is available at wileyonlinelibrary.com.]

spectra of polyacrylates synthesized at high temperature, showing the characteristic pair resonances at ≈5.5 and ≈6.5 ppm from terminal vinylidene structures (H_A and H_B in Fig. 9).[4,6] Our results indicate that H_F and H_G in MM1 that originated from DMR have chemical shifts at 5.4 and 6.6 ppm, which are probably partly responsible for the observed multiple peaks around 5.5 and 6.5 ppm in experimental ^{1}H NMR spectra.[4,6] Quan et al.[4] assigned the peaks around 126.7–128.3 ppm in ^{13}C-NMR spectrum to vinyl carbons at the end of chain (similar to C13 and C10 in macromonomer MM1 shown in Fig. 10), and the peaks next to 126.7–128.3 ppm (both downfield and upfield) to aromatic carbons. As shown in our simulated NMR spectrum of MM1 (Fig. 10), C13 (124.7 ppm) and C10 (132.4 ppm) are from the β-scission reactions, and the nearby peaks at 120.6 ppm and 139.8 correspond, respectively, to the unsaturated carbon atoms C6 and C5 of DMR. Therefore, our results suggest that the peaks at 125.4–126.0 and 137.7–137.9 ppm reported in experimental NMR spectrum[4] can be from the unsaturated carbon atoms of DMR. This indicates that both DMR and β-scission-produced live radicals can produce unsaturated chain-end carbons in the final product. It is consistent with previous studies[5,10] suggesting the capability of DMR to initiate polymerization. The agreement of computational and experimental NMR spectra points to DMR-based monomer self-initiation, propagation of DMR, and β-scission reactions in high-temperature polymerization of methyl acrylates. This approach of calculating NMR spectra via DFT-based methods allows one to effectively interpret the nature of the reacting species and underlying mechanisms. It can also be used along with the existing empirical substitute increment schemes to improve the understanding of chain distributions and transient species in a thermal polymerization processes.

Conclusions

We performed a benchmark study using high-level composite method G4(MP2)-6X to assess the performance of MP2 and

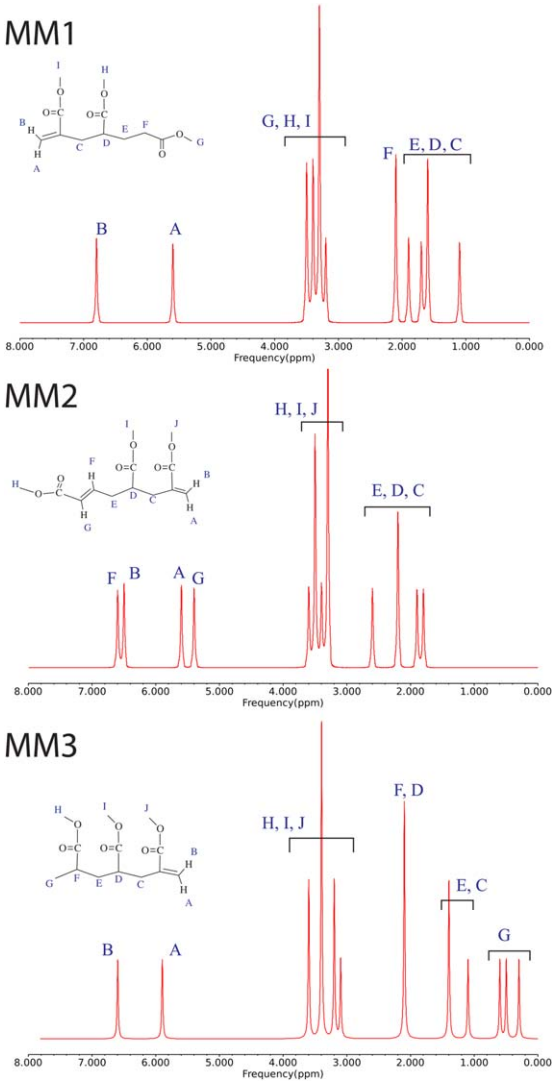

Figure 9. Simulated ^{1}H-NMR spectrums of selected macromonomers (shown in Fig. 6) using B3LYP/6-31G*. [Color figure can be viewed in the online issue, which is available at wileyonlinelibrary.com.]

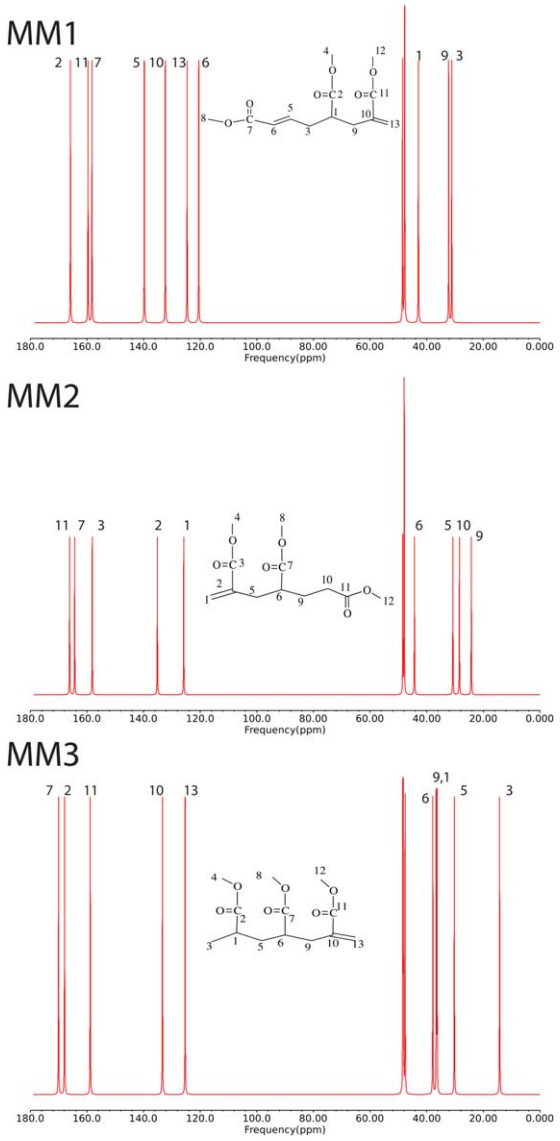

Figure 10. Simulated ^{13}C-NMR spectrums of selected macromonomers (shown in Fig. 6) using B3LYP/6-31G*. [Color figure can be viewed in the online issue, which is available at wileyonlinelibrary.com.]

Table 5. Optimized geometry of transition state for various β–scission reactions using B3LYP/6–31G*, M06–2X/6–31G*, and PBE0/6–31G*.

		B3LYP			M06–2X			PBE0		
MCR	Scheme	r_s (Å)	r_d (Å)	∠CCC	r_s (Å)	r_d (Å)	∠CCC	r_s (Å)	r_d (Å)	∠CCC
4DMCR[5]	R	2.27	1.37	109.58	2.24	1.36	104.82	2.28	1.36	107.17
5DMCR[5]	R	2.27	1.37	114.89	2.25	1.36	111.77	2.29	1.36	114.16
5DMCR[5]	L	2.28	1.37	113.79	2.26	1.36	112.55	2.24	1.37	109.18
6DMCR[5]	R	2.27	1.38	112.02	2.24	1.36	110.58	2.28	1.37	111.27
6DMCR[5]	L	2.25	1.38	109.58	2.23	1.36	105.72	2.25	1.37	108.41
3MMCR[5]	R	2.27	1.37	109.70	2.25	1.36	106.25	2.29	1.36	108.72
4MMCR[5]	R	2.25	1.38	119.01	2.25	1.38	116.35	2.27	1.37	116.64
4MMCR[5]	L	2.26	1.38	117.16	2.26	1.38	112.94	2.26	1.37	118.69
5MMCR[5]	R	2.27	1.38	112.17	2.24	1.37	109.18	2.28	1.37	111.44
5MMCR[5]	L	2.23	1.36	109.96	2.23	1.36	105.79	2.27	1.36	108.46

Table 6. Activation energy (E_a), activation free energy ($\Delta G^{\neq}_{298K}$) in kJ/mol; Wigner tunneling correction (κ_W); frequency factor (A), and rate constant (k) in s^{-1} at 298 K for β-scission reactions using B3LYP/6-31G*, M06-2X/6-31G*, and PBE0/6-31G*.

		B3LYP					M06-2X					PBE0				
MCR	Scheme	E_a	$\Delta G^{\neq}_{298K}$	lnA	κ_E	k	E_a	$\Delta G^{\neq}_{298K}$	lnA	κ_E	k	E_a	$\Delta G^{\neq}_{298K}$	lnA	κ_E	k
4DMCR[5]	R	100.03	98.72	29.99	1.22	3.84E-5	124.60	116.94	32.55	1.35	2.73E-8	119.52	107.24	34.41	1.21	1.22E-6
5DMCR[5]	R	116.23	109.59	32.14	1.21	4.75E-7	144.90	136.86	32.70	1.34	8.75E-12	137.92	140.18	28.55	1.19	2.03E-12
5DMCR[5]	L	109.09	95.19	35.07	1.21	1.57E-4	142.42	133.33	33.12	1.30	3.53E-11	131.74	120.68	33.92	1.17	5.21E-9
6DMCR[5]	R	95.07	92.19	30.62	1.24	5.41E-4	128.80	112.43	36.06	1.38	1.72E-7	117.44	120.78	28.11	1.21	5.21E-9
6DMCR[5]	L	96.19	96.81	29.21	1.24	8.40E-5	114.43	110.63	30.99	1.34	3.44E-7	116.59	125.73	25.77	1.27	7.41E-10
3MMCR[5]	R	97.69	95.27	30.43	1.22	1.54E-4	121.61	116.89	31.36	1.32	2.72E-8	120.06	118.45	30.11	1.19	1.31E-8
4MMCR[5]	R	99.09	96.31	30.58	1.30	1.08E-4	130.72	126.53	31.15	1.43	6.03E-10	124.03	115.74	32.80	1.29	4.22E-8
4MMCR[5]	L	98.68	94.08	31.31	1.23	2.51E-4	129.69	120.39	33.21	1.32	6.64E-9	123.38	116.05	32.42	1.21	3.50E-8
5MMCR[5]	R	97.76	89.62	32.74	1.25	1.54E-3	121.00	122.94	28.68	1.34	2.41E-9	117.79	109.29	32.89	1.20	5.30E-7
5MMCR[5]	L	95.90	83.36	34.52	1.24	1.92E-2	131.48	129.34	30.32	1.38	1.87E-10	118.17	100.43	36.61	1.22	1.92E-5

Table 7. Activation energy (E_a), activation free energy ($\Delta G^{\neq}_{298K}$) in kJ/mol; Wigner tunneling correction (κ_W); frequency factor (A), and rate constant (k) in s^{-1} at 298 K for β-scission reactions using B3LYP/6-31G**, M06-2X/6-31G**, and PBE0/6-31G**.

		B3LYP					M06-2X					PBE0				
MCR	Scheme	E_a	$\Delta G^{\neq}_{298K}$	lnA	κ_E	k	E_a	$\Delta G^{\neq}_{298K}$	lnA	κ_E	k	E_a	$\Delta G^{\neq}_{298K}$	lnA	κ_E	k
4DMCR[5]	R	99.98	98.00	30.25	1.22	5.12E-5	123.70	108.29	35.67	1.34	8.88E-7	119.63	114.76	31.42	1.20	5.83E-8
5DMCR[5]	R	115.06	107.83	32.38	1.21	9.67E-7	143.05	123.41	37.38	1.34	1.99E-9	136.08	135.05	29.88	1.19	1.61E-11
5DMCR[5]	L	108.81	98.63	33.57	1.21	3.95E-5	140.83	122.05	37.03	1.30	3.33E-9	130.19	117.21	34.69	1.17	2.11E-8
6DMCR[5]	R	94.70	91.26	30.84	1.23	7.86E-4	128.13	106.93	38.01	1.38	1.58E-6	116.90	114.88	30.27	1.21	5.63E-8
6DMCR[5]	L	95.63	95.96	29.32	1.23	1.18E-4	113.57	101.29	34.41	1.33	1.49E-5	115.87	119.88	27.84	1.27	7.85E-9
3MMCR[5]	R	97.85	96.19	30.13	1.22	1.06E-4	120.54	111.37	33.16	1.32	2.52E-7	120.02	119.76	29.56	1.19	7.72E-9
4MMCR[5]	R	98.32	95.10	30.76	1.29	1.75E-4	129.57	121.89	32.56	1.42	3.90E-9	122.62	115.28	32.42	1.29	5.08E-8
4MMCR[5]	L	98.01	93.52	31.27	1.23	3.15E-4	128.37	117.79	33.73	1.33	1.90E-8	121.92	115.61	32.00	1.21	4.18E-8
5MMCR[5]	R	96.89	89.93	32.27	1.25	1.36E-3	119.42	113.32	31.92	1.33	1.16E-7	116.57	108.86	32.57	1.20	6.30E-7
5MMCR[5]	L	95.32	83.68	34.15	1.24	1.68E-2	129.93	119.30	33.74	1.37	1.07E-8	117.37	101.84	35.72	1.22	1.09E-5

three types of density functionals, B3LYP, M06-2X, and PBE0 with various basis sets on backbiting reactions. The RRHO and HR approximations were applied to estimate frequency factors. It was found that both B3LYP and M06-2X perform well for calculating energy barriers of backbiting reactions. We determined that the frequency factors calculated using the RRHO and HR approximations differ by a factor of 2. The estimated rate constant agrees with values obtained using macroscopic modeling and sample measurements from laboratory experiments and the DFT calculations from other groups.[42,44,45] The activation energies and kinetic constants of 1:3, 1:5, 1:7, and 1:9 backbiting reactions free-radical polymerization of methyl acrylate were computed using B3LYP/6-31G*, M06-2X/6-31G* and PBE0/6-31G* for live chains with difference lengths. The

Table 8. Calculated and experimental ^{13}C chemical shifts of dead polymer chains affected by backbiting and β–scission reactions.

Description	Details	Calculated Peaks	Experimental Peaks[4]
CH_2's on backbone	CH_2 prior to the saturated CH_2 on end group	25.5–27.9	27.1–29.6
	CH_2, saturated end group	29.3–31.5	31.8
	CH_2, methylene group in backbone	31.3–37	33.2–37
	CH_2, methylene group next to the branch point	31.3–43.2	37–37.9
CH's in backbone	Methine group in backbone, CH next to the branch point	36.8–43.5	37.9–39.4
	Methine group in backbone, CH	40–41.6	41.1–42.5
Carbonyl C's	COOX next to terminal unsaturation	157.6–158.8 (X = CH_3)	166.4–166.7 (X = CH_2CH_3)
	COOX next to terminal saturation	165.1–167.9 (X = CH_3)	172.7–172.9 (X = CH_2CH_3)
	COOX in backbone	166.6–172.6 (X = CH_3)	172.9–175.4 (X = CH_2CH_3)
Branch point C's	Quarternary carbon's in backbone	50.6–54.5	47.8–48.3
Vinyl C's	In–chain vinyl C at the end of the chain	119.3–122.4	125.4–126.0
	Terminal vinyl C at the end of the chain	124.7–125.9	126.7
	Terminal vinyl C at the end of the chain	132.4–135.2	127.8–128.3
	In–chain vinyl C at the end of the chain	139.0–140.3	128.9–137.9
CH_3's	C in O–CH_3	47–48.3	–
	C in the end group CH_3	13–21.3	–
	C in the CH_3 near the branch point	21.3	–

1:5 and 1:7 backbiting mechanisms are energetically favorable compared to 1:3 and 1:9 backbiting mechanisms. Moreover, the chain length may influence the kinetic favorability of remote hydrogen transfer reactions, such as the 1:7 backbiting reaction. The kinetics of the reactions were further validated using B3LYP/6-31G**, M06-2X/6-31G**, and PBE0/6-31G**. The size of the basis set was found to have no significant effect on the predicted values within our study. The chemical shifts of carbon nuclei in various final products were predicted using B3LYP/6-31G*, and the predicted chemical shifts are comparable to those obtained from spectroscopic polymer sample analyses. The predicted chemical shifts were used to determine the molecular structure of reactants, products, and transitions states in backbiting and β-scission reactions. The β-scission reactions of MCRs from 1:5 backbiting for the R-side and L-side β-scissions were found to have comparable activation energies, and the energy barriers are not dependent on the polymer chain length. The NMR spectra calculated with B3LYP/6-31G* agree with experimental results, which further validates the proposed mechanisms. The application of state-of-art first-principles method, G4(MP2)-6X, still results in larger activation energy compared to macroscopic-modeling-based experimental values, suggesting a need for (1) further theoretical studies of these reactions using a more realistic model including the solvent effect and (2) the refinement of mechanistic reaction models.

Acknowledgments

Computational support was provided by the High-Performance Computing Modernization Office of the U.S. Department of Defense.

Keywords: methyl acrylate · backbiting · β-scission · midchain radical · density functional theory

How to cite this article: S. Liu, S. Srinivasan, M. C. Grady, M. Soroush, A. M. Rappe, *Int. J. Quantum Chem.* **2014**, *114*, 345–360. DOI: 10.1002/qua.24572

Additional Supporting Information may be found in the online version of this article.

[1] K. Adamsons, G. Blackman, B. Gregorovich, L. Lin, R. Matheson, *Prog. Org. Coat.* **1998**, *34*, 64.
[2] P. A. Sorensen, S. Kiil, K. Dam-Johansen, C. E. Weinell, *J. Coat. Technol. Res.* **2009**, *6*, 135.
[3] M. C. Grady, W. J. Simonsick, R. A. Hutchinson, *Macromol. Symp.* **2002**, *182*, 149.
[4] C. L. Quan, M. Soroush, M. C. Grady, J. E. Hansen, W. J. Simonsick, *Macromolecules* **2005**, *38*, 7619.
[5] S. Srinivasan, M. W. Lee, M. C. Grady, M. Soroush, A. M. Rappe, *J. Phys. Chem. A* **2009**, *113*, 10787.
[6] J. Chiefari, J. Jeffery, R. T. A. Mayadunne, G. Moad, E. Rizzardo, S. H. Thang, *Macromolecules* **1999**, *32*, 7700.
[7] A. M. Zorn, T. Junkers, C. Barner-Kowollik, *Macromol. Rapid Commun.* **2009**, *30*, 2028.
[8] S. Srinivasan, M. W. Lee, M. C. Grady, M. Soroush, A. M. Rappe, *J. Phys. Chem. A* **2010**, *114*, 7975.
[9] S. Srinivasan, M. W. Lee, M. C. Grady, M. Soroush, A. M. Rappe, *J. Phys. Chem. A* **2011**, *115*, 1125.
[10] S. Srinivasan, G. Kalfas, V. I. Petkovska, C. Bruni, M. C. Grady, M. Soroush, *J. Appl. Polym. Sci.* **2010**, *118*, 1898.
[11] T. Junkers, C. Barner-Kowollik, *J. Polym. Sci. Part A: Polym. Chem.* **2008**, *46*, 7585.
[12] A. M. van Herk, *Macromol. Rapid Commun.* **2009**, *30*, 1964.
[13] D. Lim, O. Wichterle, *J. Polym. Sci.* **1958**, *29*, 579.
[14] M. J. Roedel, *J. Am. Chem. Soc.* **1953**, *75*, 6110.
[15] D. Britton, F. Heatley, P. A. Lovell, *Macromolecules* **1998**, *31*, 2828.
[16] N. M. Ahmad, D. Britton, F. Heatley, P. A. Lovell, *Macromol. Symp.* **1999**, *143*, 231.
[17] F. Heatley, P. A. Lovell, T. Yamashita, *Macromolecules* **2001**, *34*, 7636.
[18] N. M. Ahmad, B. Charleux, C. Farcet, C. J. Ferguson, S. G. Gaynor, B. S. Hawkett, F. Heatley, B. Klumperman, D. Konkolewicz, P. A. Lovell, K. Matyjaszewski, R. Venkatesh, *Macromol. Rapid Commun.* **2009**, *30*, 2002.
[19] M. Azukizawa, B. Yamada, D. J. T. Hill, P. J. Pomery, *J. Macromol. Chem. Phys.* **2000**, *201*, 774.
[20] B. Yamada, M. Azukizawa, H. Yamazoe, D. J. T. Hill, P. J. Pomery, *Polymer* **2000**, *41*, 5611.
[21] J. Barth, M. Buback, P. Hesse, T. Sergeeva, *Macromol. Rapid Commun.* **2009**, *30*, 1969.
[22] T. Junkers, F. Bennet, S. P. S. Koo, C. Barner-Kowollik, *J. Polym. Sci. Part A: Polym. Chem.* **2008**, *46*, 3433.
[23] B. Yamada, F. Oku, T. Harada, *J. Polym. Sci. Part A: Polym. Chem.* **2003**, *41*, 645.
[24] J. M. Asua, S. Beuermann, M. Buback, P. Castignolles, B. Charleux, R. G. Gilbert, R. A. Hutchinson, J. R. Leiza, A. N. Nikitin, J. P. Vairon, A. M. van Herk, *Macromol. Chem. Phys.* **2004**, *205*, 2151.
[25] W. Wang, R. A. Hutchinson, *Chem. Eng. Technol.* **2010**, *33*, 1745.
[26] A. N. Nikitin, R. A. Hutchinson, W. Wang, G. A. Kalfas, J. R. Richards, C. Bruni, *Macromol. React. Eng.* **2010**, *4*, 691.
[27] A. N. Nikitin, R. A. Hutchinson, G. A. Kalfas, J. R. Richards, C. Bruni, *Macromol. Theory Simul.* **2009**, *18*, 247.
[28] A. N. Nikitin, R. A. Hutchinson, *Macromol. Rapid Commun.* **2009**, *30*, 1981.
[29] A. N. Nikitin, R. A. Hutchinson, M. Buback, P. Hesse, *Macromolecules* **2007**, *40*, 8631.
[30] A. N. Nikitin, R. A. Hutchinson, *Macromol. Theory Simul.* **2006**, *15*, 128.
[31] A. N. Nikitin, R. A. Hutchinson, *Macromolecules* **2005**, *38*, 1581.
[32] C. L. Zhang, X. Y. Wang, L. M. Liu, Y. L. Wang, X. Y. Peng, *J. Mol. Model.* **2008**, *14*, 1053.
[33] I. Degirmenci, V. Aviyente, V. Van Speybroeck, M. Waroquier, *Macromolecules* **2009**, *42*, 3033.
[34] V. Van Speybroeck, K. Van Cauter, B. Coussens, M. Waroquier, *ChemPhysChem* **2005**, *6*, 180.
[35] T. Furuncuoglu, I. Ugur, I. Degirmenci, V. Aviyente, *Macromolecules* **2010**, *43*, 1823.
[36] X. R. Yu, S. E. Levine, L. J.. Broadbelt, *Macromolecules* **2008**, *41*, 8242.
[37] X. R. Yu, J. Pfaendtner, L. J. Broadbelt, *J. Phys. Chem. A* **2008**, *112*, 6772.
[38] H. Gunaydin, S. Salman, N. S. Tuzun, D. Avci, V. Aviyente, *Int. J. Quant. Chem.* **2005**, *103*, 176.
[39] V. Tognett, P. Cortona, C. Adamo, *Int. J. Quant. Chem.* **2010**, *110*, 2320.
[40] M. Dossi, G. Storti, D. Moscatelli, *Macromol. Theory Simul.* **2010**, *19*, 170.
[41] I. Yavuz, G. A. A. Ciftcioglu, *Comput. Theor. Chem.* **2011**, *978*, 88.
[42] X. R. Yu, L. J. Broadbelt, *Macromol. Theory Simul.* **2012**, *21*, 461.
[43] S. Liu, S. Srinivasan, M. C. Grady, M. Soroush, A. M. Rappe, In AIChE Annual Meeting, Pittsburgh, PA, **2012**.
[44] D. Cuccato, E. Mavroudakis, M. Dossi, D. Moscatelli, *Macromol. Theory Simul.* **2013**, *22*, 127.
[45] D. Cuccato, E. Mavroudakis, D. Moscatelli, *J. Phys. Chem. A* **2013**, *117*, 4358.
[46] J. Barth, M. Buback, P. Hesse, T. Sergeeva, *Macromolecules* **2010**, *43*, 4023.
[47] K. Burke, *Phys. Chem.* **2012**, *136*, 150901.

[48] F. Jansen, Introduction to Computational Chemistry; Wiley: Chichester, England, **2007**.
[49] B. Chan, J. Deng, L. Radom, *J. Chem. Theory Comput.* **2011**, *7*, 112.
[50] B. Chan, L. Radom, *J. Phys. Chem. A* **2012**, *116*, 4975.
[51] A. D. Becke, *J. Chem. Phys.* **1993**, *98*, 5648.
[52] R. H. Hertwig, W. Koch, *Chem. Phys. Lett.* **1997**, *268*, 345.
[53] P. J. Stephens, F. J. Devlin, C. F. Chabalowski, M. J. Frisch, *J. Phys. Chem.* **1994**, *98*, 11623.
[54] Y. Zhao, D. G. Truhlar, *J. Org. Chem.* **2007**, *72*, 295.
[55] Y. Zhao, D. G. Truhlar, *Theor. Chem. Acc.* **2008**, *120*, 215.
[56] C. Adamo, V. Barone, *J. Chem. Phys.* **1999**, *110*, 6158.
[57] J. Pfaendtner, X. Yu, L. J. Broadbelt, *Theor. Chem. Acc.* **2007**, *118*, 881.
[58] C. Y. Lin, E. I. Izgorodina, M. L. Coote, *J. Phys. Chem. A* **2008**, *112*, 1956.
[59] M. L. Coote, *J. Phys. Chem. A* **2005**, *109*, 1230.
[60] P. Vansteenkiste, V. Van Speybroeck, G. B. Marin, M. Waroquier, *J. Phys. Chem. A* **2003**, *107*, 3139.
[61] M. J. Frisch, G. W. Trucks, H. B. Schlegel, G. E. Scuseria, M. A. Robb, J. R. Cheeseman, G. Scalmani, V. Barone, B. Mennucci, G. A. Petersson, H. Nakatsuji, M. Caricato, X. Li, H. P. Hratchian, A. F. Izmaylov, J. Bloino, G. Zheng, J. L. Sonnenberg, M. Hada, M. Ehara, K. Toyota, R. Fukuda, J. Hasegawa, M. Ishida, T. Nakajima, Y. Honda, O. Kitao, H. Nakai, T. Vreven, J. A. Montgomery, Jr., J. E. Peralta, F. Ogliaro, M. Bearpark, J. J. Heyd, E. Brothers, K. N. Kudin, V. N. Staroverov, R. Kobayashi, J. Normand, K. Raghavachari, A. Rendell, J. C. Burant, S. S. Iyengar, J. Tomasi, M. Cossi, N. Rega, J. M. Millam, M. Klene, J. E. Knox, J. B. Cross, V. Bakken, C. Adamo, J. Jaramillo, R. Gomperts, R. E. Stratmann, O. Yazyev, A. J. Austin, R. Cammi, C. Pomelli, J. W. Ochterski, R. L. Martin, K. Morokuma, V. G. Zakrzewski, G. A. Voth, P. Salvador, J. J. Dannenberg, S. Dapprich, A. D. Daniels, O. Farkas, J. B. Foresman, J. V. Ortiz, J. Cioslowski, D. J. Fox, R. A. Gaussian 09, Revision D.01; Gaussian, Inc.; Wallingford, CT, **2009**.
[62] M. W. Schmidt, K. K. Baldridge, J. A. Boatz, S. T. Elbert, M. S. Gordon, J. H. Jensen, S. Koseki, N. Matsunaga, K. A. Nguyen, S. J. Su, T. L. Windus, M. Dupuis, J. A. Montgomery, *J. Comput. Chem.* **1993**, *14*, 1347.
[63] M. W. Wong, L. Radom, *J. Phys. Chem.* **1995**, *99*, 8582.
[64] M. W. Wong, L. Radom, *J. Phys. Chem. A* **1998**, *102*, 2237.
[65] Y. Y. Chuang, E. L. Coitino, D. G. Truhlar, *J. Phys. Chem. A* **2000**, *104*, 446.
[66] M. L. Coote, *Encycl. Polym. Sci. Technol.* **2006**, 1.
[67] C. Eckart, *Phys. Rev.* **1930**, *35*, 1303.
[68] H. Eyring, *J. Chem. Phys.* **1935**, *3*, 107.
[69] E. P. Z. Wigner, *Phys. Chem.* **1932**, *19*, 203.
[70] S. Liu, S. Srinivasan, M. C. Grady, M. Soroush, A. M. Rappe, *J. Phys. Chem. A* **2012**, *116*, 5337.
[71] W. Kutzelnigg, *Isr. J. Chem.* **1980**, *19*, 193.
[72] M. Schindler, W. Kutzelnigg, *J. Chem. Phys.* **1982**, *76*, 1919.
[73] F. Neese, The ORCA program system. *WIREs Comput Mol Sci*. **2012** *2*, 73.
[74] C. Y. Lin, E. I. Izgorodina, M. L. Coote, *Macromolecules* **2010**, *43*, 553.
[75] D. Cuccato, M. Dossi, D. Moscatelli, G. Storti, *Macromol. React. Eng.* **2012**, *6*, 330.
[76] D. Cuccato, M. Dossi, D. Polino, C. Cavallotti, D. Moscatelli, *Macromol. React. Eng.* **2012**, *6*, 496.
[77] D. Moscatelli, C. Cavallotti, M. Morbidelli, *Macromolecules* **2006**, *39*, 9641.
[78] Y. Zhao, D. G. Truhlar, *Acc. Chem. Res.* **2008**, *41*, 157.
[79] R. Jain, T. Bally, P. R. Rablen, *J. Org. Chem.* **2009**, *74*, 4017.
[80] K. W. Wiitala, T. R. Hoye, C. J. Cramer, *J. Chem. Theory Comput.* **2006**, *2*, 1085.

Received: 23 August 2013
Revised: 30 September 2013
Accepted: 10 October 2013
Published online 19 November 2013